IEEE Access
Multidisciplinary ⋮ Rapid Review ⋮ Open Access Journal

Received March 26, 2022, accepted April 14, 2022, date of publication April 18, 2022, date of current version April 28, 2022.

Digital Object Identifier 10.1109/ACCESS.2022.3168650

A Novel Control Strategy of Phase-Controlled Switching Technology for Vacuum Circuit Breaker

AIMIN LIU[1], (Member, IEEE), ZHIHENG WU[1,2], (Member, IEEE), YUCHEN WANG[1], (Member, IEEE), AND SHAOHUA MA[1], (Member, IEEE)

[1]Department of Electrical Engineering, Shenyang University of Technology, Shenyang 110178, China
[2]Zhengzhou Zhengfei Special Equipment Company Ltd., Zhengzhou 451475, China

Corresponding author: Zhiheng Wu (kf.wujing@163.com)

ABSTRACT The opening and closing of a vacuum circuit breaker in the selected phase of the system voltage and the associated electrical equipment plug in or disconnect the electrical system with minimal impact on itself and the system. To realize this and ensure the control precision and stability of its action process, this study designs the drive motor and controller of a vacuum circuit breaker actuator. Additionally, a new function-switching pseudo-differential control (FPD) strategy is based on the feedback element principle. The control strategy avoids the direct differentiation of the controlled variables and has the ability of a fast dynamic response and anti-interference. At the same time, according to the moving process of the circuit breaker contacts, the control parameters are directly assigned to the system in stages, which reduces the amount of calculation and enhances the response speed of the control system. According to the research on the motor actuator movement process, the motor actuator and its control system of a 40.5 kV vacuum circuit breaker are developed and verified by closing operation in the selected phase, and the experimental results show the effectiveness of the proposed control strategy.

INDEX TERMS Permanent magnet motor, FPD, actuator, vacuum circuit breaker.

I. INTRODUCTION

Intelligent high-voltage electrical appliances are an inevitable trend in the development of power systems. A high-voltage vacuum circuit breaker (VCB) is one of the most important pieces of equipment in power system [1], [2]. Phase-controlled switching technology, as the core content of intelligent high-voltage electrical appliances, is a research hotspot in this field and is also one of the key technologies in the construction of smart power grids. In the International Council on Large Electric Systems (CIGRE), researchers analyzed and discussed the phase-controlled switching technology of high-voltage electrical appliances and proposed that the opening and closing accuracy should be within ±1ms.

The traditional actuator of high-voltage VCB adopts spring, hydraulic, or pneumatic technology with many linkages and complex structures [3]–[5]. Therefore, it has a large tolerance of accumulated movement, slow response, and poor control, and it is difficult to realize the movement control of contacts and achieve the precision requirements of the VCB phase-controlled switching technology. The motor actuator is a new type of VCB actuator that simplifies its moving parts and improves its reliability compared to a traditional actuator in a structure. In the control mode, the power electronic technology drives the motor to drive the mechanism action, which is highly controllable and provides the possibility for phase-controlled switching technology of the VCB. Precise control of the actuator driving motor is the key to realizing phase-controlled switching technology of the VCB.

In recent years, domestic and foreign scholars have conducted extensive research on the control methods for drive motors. The control of permanent magnet motors is diverse and intelligent [6]. Reference [7] proposed a PMSM drive using a hybrid PI speed controller with inherent and noninherent switching functions. The combined advantages of these two controllers can be obtained using a hybrid fuzzy PI speed controller. Reference [8] proposed a novel model predictive control for a three-phase permanent-magnet synchronous

The associate editor coordinating the review of this manuscript and approving it for publication was Wonhee Kim.

motor (PMSM) with enhanced robustness against parameter variations and higher current control precision. To enhance the speed control performance of a permanent magnet synchronous motor (PMSM) with internal and external disturbances, a new adaptive terminal sliding mode reaching law (ATSMRL) was proposed with continuous fast terminal sliding mode control (CFTSMC) in reference [9]. Moreover, many optimization control methods were proposed in reference [10]–[20] for the application of motors in different fields.

The aforementioned control strategies have realized optimal control of the motor in different fields and achieved certain results. However, when the motor was applied to the VCB actuator, its working time was only approximately 40ms, and the speed and torque changed significantly. The above control algorithms are difficult to directly quote. The motor control in the VCB actuator must consider different load, speed and closing time requirements. At present, research on motor control in VCB actuators is gradually increasing. Reference [21] proposed that a VCB motor actuator adopts constant-torque control, and its control accuracy is less than 1ms after conversion. A fuzzy adaptive PID control strategy was proposed for a VCB motor actuator in reference [22]. The control strategy has a good tracking accuracy; however, no specific precision value is provided.

In view of the above problems, based on the discussion of the feedback principle, this study proposes an FPD control strategy for the motor control system, which combines conventional and intelligent control ideas and provides a new control algorithm with appropriate control parameters according to segmented environmental changes. This solves the problem that the traditional control algorithm cannot adjust its parameters according to the environment while settling the problem of the intelligent control algorithm adjusting control parameters because of the redundant and complex calculation affecting the response speed. The pseudo-differential algorithm solves the problem in which the controlled variable is directly differentiated in the conventional PID control algorithm, in which the output varies with the integral and differential of the input but cannot closely follow the change in the input. The new control algorithm ensures that the system has the ability of fast following and anti-interference capabilities. The feasibility of the control method is verified through simulations and experimental results.

II. MOTOR ACTUATOR OF CIRCUIT BREAKER

A. MOTION CHARACTERISTIC ANALYSIS OF MOTOR ACTUATOR AND MOTOR DESIGN

The dynamic characteristics of 40.5 kV VCB are the load characteristics of the motor actuator; therefore, analysis of the dynamic characteristics is a necessary condition for the design of the optimal motor actuator. The closing operation is much more complicated than the opening operation, and the opening operation is only the reverse process of the former, so the closing operation is the main research topic

TABLE 1. The technical parameter of 40.5 kV VCB.

Name	Value	Name	Value
the distance of the contact(mm)	25±3	the over-range(mm)	8±3
average closing speed (m/s)	≥0.8±0.2	average opening speed (m/s)	≥2.0±0.3
contact self closing force (Nm)	200±30	contact counter-force (N)	300±30
bouncing time of contact (ms)	□3	switching synchronization (ms)	□2
mass of moving parts (kg)	4	contact pressure rating (Nm)	2900±300

of this paper, in which the studied VCB model is TD-40.5/1600-31.5. The main technical parameters of this model VCB in Table 1 [23]. The structure of the 40.5 kV VCB motor actuator is shown in Fig. 1.

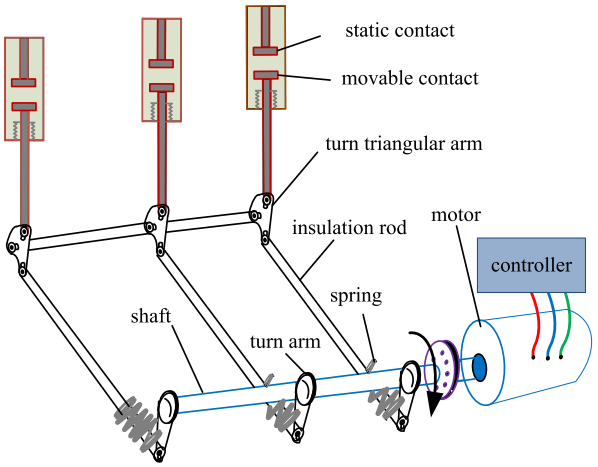

FIGURE 1. Structure schematic of VCB motor actuator.

When the VCB is closed, the motor rotates to drive the linking mechanism of the circuit breaker and realize the closing operation of the switch contact. The opening operation was the opposite of the movement process. The relationships between the motor rotation angle, contact distance, and load torque during the VCB closing process are shown in Fig. 2.

In the closing process, the motor rotation angle was between 0°-42°, and the motor actuator drove the VCB contacts to move within a distance of 25 mm. This stage is defined as the travel stage. The over-range motion process of the compression spring after the contact of the movable and static contacts is 42°–62 °, and the over-range is 8 mm. This stage was defined as the overtravel stage. The load counter-torque is small in the travel stage; therefore, the motor actuator is not necessary to output a large torque at this stage. The contact spring is compressed when the motor turns 42°, and the load counter-torque is abruptly increased to 330 Nm; hence, the motor actuator output torque should be high to overcome the force of the contact spring.

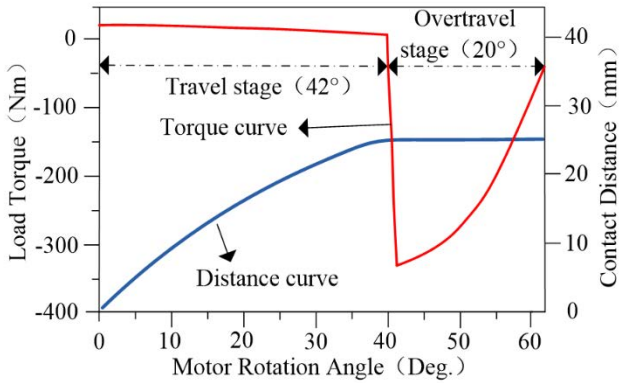

FIGURE 2. Corresponding relation between motor rotation angle contact distance and load torque.

TABLE 2. Driving motor design parameters.

Project	Value	Project	Value
pole-pairs	2	each slot number of turns	20
phase resistance/Ω	0.8	stator inner diameter/mm	105
stator outer diameter/mm	170	permanent magnet thickness/mm	10
armature core length/mm	400	rotor diameter/mm	44
rotor outside diameter/mm	94	radian of permanent magnet block	84
external diameter of permanent magnet/mm	104	inner diameter of permanent magnet/mm	94
slot number	36	number of slots per pole per phase	3
permanent magnet materials	N40SH	spindle materials	40Cr
stator material	DW470	rotor material	10#steel

In the VCB motor actuator, the drive motor converts electrical energy into mechanical energy and drives the contact movement via the transmission mechanism. The performance of the drive motor to satisfy the requirements of the VCB motion characteristics is the premise for realizing a phase-controlled closing operation. Therefore, the drive motor of the actuator should have a fast starting speed, large starting torque, short mechanical response time, high working reliability and operational stability. Consequently, it is necessary to design a drive motor that can satisfy the operating characteristics of the VCB. The basic structural parameters of the designed motor are presented in Table 2 [1].

The motor design is illustrated in Fig. 3. The paragraph below focuses on the two conditions for the analysis of its dynamic characteristics. Fig. 4 shows the motor magnetic density distribution and air-gap magnetic density distribution when the motor winding current is zero. It can be seen from the motor magnetic density distribution diagram that the rotor yoke and stator yoke magnetic density is relatively large, the maximum magnetic density can reach 1.8-2.4T. Fig. 5 shows the magnetic density distribution of the motor and the air gap when the motor winding current is at its maximum. It can be seen that, owing to the superposition of the winding current and magnetic field, the maximum magnetic density can reach 2.3T, and the magnetic circuit of the motor is between 1.2 and 1.6T. The average air gap flux density is 0.9T, which meets the requirements of the high magnetic load design goal of the driving motor.

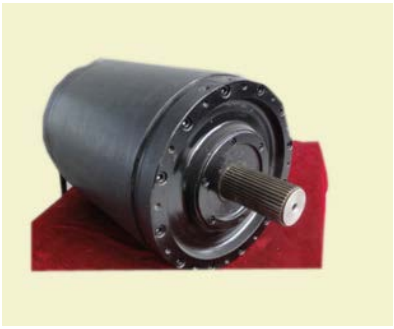

FIGURE 3. Physical picture of motor.

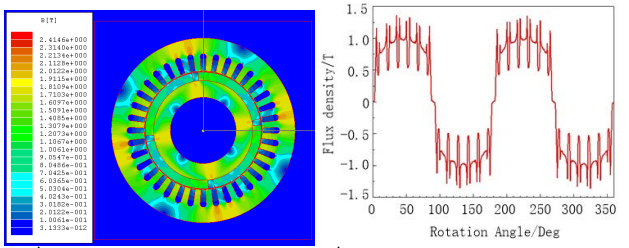

a) Magnetic density distribution b) Air gap flux density distribution

FIGURE 4. Magnetic field distribution of the motor when the current is zero.

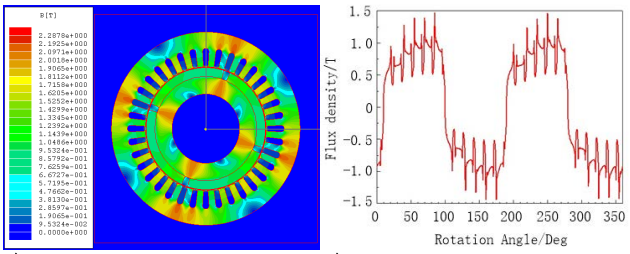

a) Magnetic density distribution b) Air gap flux density distribution

FIGURE 5. Magnetic field distribution of motor at maximum current.

Open-loop simulation experiments are conducted to verify the accuracy and effectiveness of the motor model. The output current, electromagnetic torque, back EMF, and speed performance curves of the motor were analyzed, which laid the foundation for the next closed-loop control simulation of the motor. The operating voltage was set at 200V. A variable step size ODE45 simulation method was adopted, and the simulation time was set to 0.15s. The open-loop simulation

model of the motor and the simulation results are shown in Fig. 6.

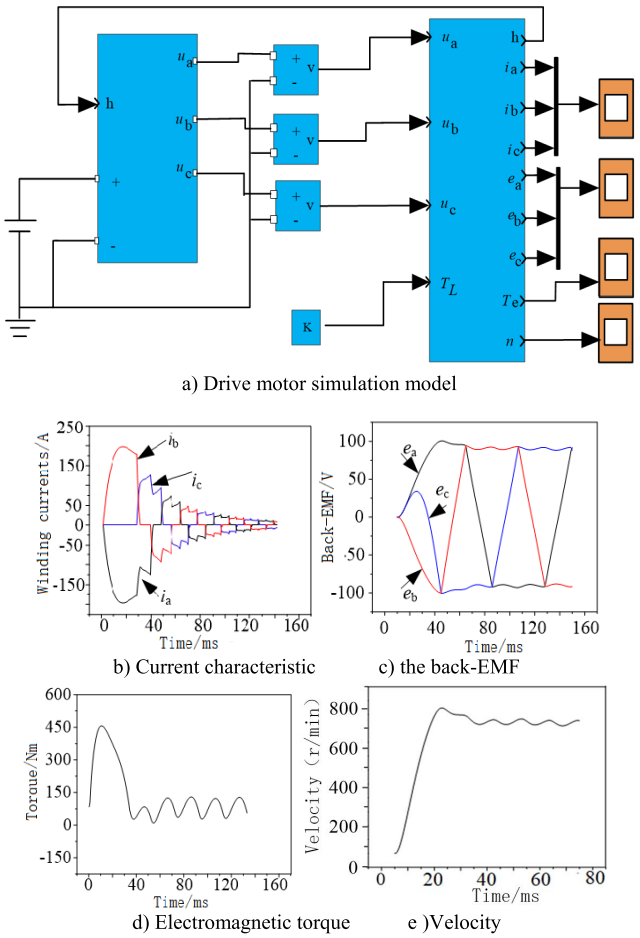

FIGURE 6. Motor characteristic curve.

According to the motor simulation results, the maximum winding current was 190A when the motor started, which was in line with the current output range requirements. The back-EMF waveform output was similar to that of the trapezoidal wave, and the width of the flat top wave was close to 120°, satisfying the back-EMF waveform output in the ideal state. The maximum output electromagnetic torque of the motor is 450 N/m, which satisfies the requirements of the VCB load torque. The maximum speed of the motor is 800r/min, which meets the requirements of the VCB closing maximum speed of 2.5±0.2 m/s (i.e., converted to the motor side is 706r/min). Therefore, the designed motor meets the technical requirements of a 40.5 kV VCB.

B. PHASE-CONTROLLED CLOSING TECHNOLOGY

Phase-controlled closing technology refers to the closing operation of a VCB at a specified phase of the grid voltage. In this study, the zero-phase closing operation of a VCB was studied. When the VCB and related equipment are placed in the power grid at the zero phase, the impact of the inrush current and overvoltage on the power equipment and system during the closing operation can be reduced, and the power quality of the system can be improved. According to the analysis, it is necessary to ensure precise control of the switch contact speed in the stroke stage to realize the zero-phase closing operation of the VCB in the grid voltage. Because the motor rotation angle can directly reflect the closing movement process of the VCB switch contact, this study analyzes zero-phase closing technology through the motor rotation angle.

The VCB motor actuator control system receives the closing instruction and calculates the time required for the motor actuator to close at the zero phase of the grid voltage according to the collected current grid voltage value. The required rotation speed and angle of the motor actuator within the required time were calculated successively, and the reference preset curve is shown in Fig. 7. The control system adjusts the speed according to the preset reference and feedback signals in real time, allowing the motor rotor to be in the zero phase of the grid voltage when it rotates at 42°.

During the VCB closing process, the motor actuator started to stop, the angle of rotation was 62°, the actuation time was tens of milliseconds, and the torque varied from moment to moment because it overcame the reverse power of the transmission mechanism. Therefore, the control strategy must have fast response and anti-interference abilities.

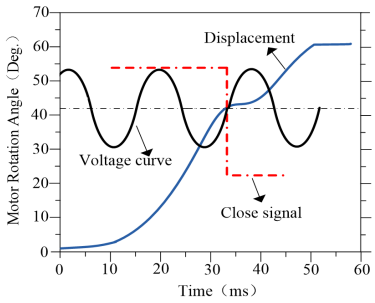

FIGURE 7. Preset reference curve of zero-phase closing.

III. FUNCTION-SWITCHING PSEUDO-DIFFERENTIAL CONTROL STRATEGY

A. THEORETICAL ANALYSIS AND DESIGN OF FUNCTION-SWITCHING PSEUDO-DIFFERENTIAL CONTROL STRATEGY

To realize the phase-controlled closing technology analyzed above, it is necessary to solve the problem of ensuring the control precision of the driving motor within a short period of time when the speed changes significantly. In the conventional PID control strategy, the parameters are fixed and cannot satisfy the requirements of the control performance under changing environments. The intelligent control algorithm can adjust the control parameters in real time, but it requires complex calculations, which directly affect the speed of the control strategy. The VCB closing process is approximately 40ms, so this cannot be guaranteed. To solve this practical engineering problem, an innovative function-switching

pseudo-differential control strategy is designed to implement phase-controlled closing technology. The new control strategy has the characteristics of strong anti-interference ability, small overshoot, and fast response, which ensures that the control system can achieve real-time and accurate control of the motor mechanism. The principle diagram is shown in Fig. 8.

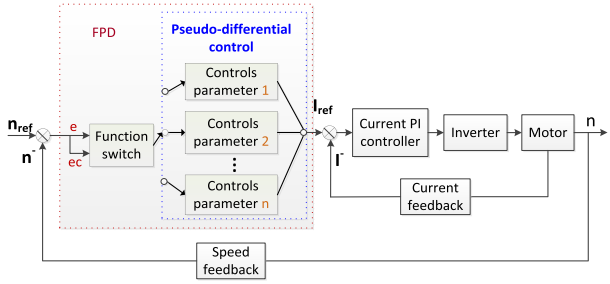

FIGURE 8. The principle diagram of the function-switching pseudo-differential control strategy.

To ensure that the control system can obtain the optimal control parameters in each speed stage without many calculations, the idea of the switching function is to directly provide the optimal control parameters to the motor actuator according to its stage. By analyzing the operation characteristics of the VCB, the speed adjustment can be divided into five stages: acceleration 1, uniform speed, acceleration 2, deceleration and closing position during the closing process. The deviation value, target value and realization time of the five stages of the analysis are listed in Table 3.

TABLE 3. The deviation value, target value and realization time of the five stages.

Stages	Deviation value	Target value	Realization time
acceleration 1	1.2m/s	1.2m/s	10ms
uniform speed	0.1m/s	1.3m/s	5ms
acceleration 2	0.9m/s	2.2m/s	20ms
deceleration	-2m/s	0.2m/s	15ms
close position	-0.2m/s	0m/s	5ms

During the implementation process, the sampling period to 1ms. In the acceleration 1 stage, the contact speed of the VCB was accelerated from 0 to 1.2 m/s in 10 ms. At this stage, the slope of the velocity increase was 0.12. Because the given value is a velocity curve, the deviation at each sampling moment should be 0.12 m/s. The absolute value of the deviation is large, so it only needs to open the loop to implement strong proportional control.

In the uniform speed phase, the deviation was less than 0.02 m/s. The current speed should be maintained and the error should be eliminated. At this point, we set the smaller value of the proportional coefficient and the moderate value of the integral and differential values.

In the acceleration 2 phase, the total deviation is 0.9 m/s. The speed increase time is 20ms. The velocity growth slope is 0.045. In this stage, the speed finally reaches a maximum value. However, the deviation tended to decrease. To avoid overshoot, the proportional coefficient was set to a moderate scale value, and the integral and differential were set to small values.

In the deceleration stage, the maximum speed is reduced to 0.2 m/s in 15 ms, with a speed decline slope of about 0.13 m/s.The speed deviation was large. At this stage, a larger proportion value is set, and smaller integral and differential values are set.

In the fifth stage, the speed was reduced to 0 within 5ms. The absolute value of the error is very small. At this time, a strong integration link was added to gradually eliminate the static difference. The proportion parameter was set to small, the integral parameter was set to large, and the differential was set to 0.

The preliminary selection of parameters in each stage was based on the actual running state, expert knowledge, operating experience, and control law of the contact. The control parameters of the five stages are K_{pj}, K_{ij}, *and* K_{dj} *(j=1,2,3,4,5)*. After the parameters are determined, they are further adjusted during the switching stage. In the closing process, the controller obtains the indicator information of the VCB at sampling time (contact speed, c; contact stroke, d; running time, t). When the preset reference speed is v and the contact stroke *is* s, the velocity error is $e_{(k)} = v_{(k)} - c_{(k)}$, the contact stroke deviation is $\Delta s = s_{(k)} - d_{(k)}$, *and* k is the sampling moment. The adjustment rules for the control parameters are as follows.

If $e_{(k)} > 0, \Delta s > 0, \Delta K_{pj(k)} = K_1 \times \Delta K_{pj(k-1)}$.

If $e_{(k)} < 0, \Delta s > 0, \Delta K_{pj(k)} = K_2 \times \Delta K_{pj(k-1)}, \Delta K_{i(k)} = I_2 \times \Delta K_{ij(k-1)}, \Delta K_{dj(k)} = D_2 \times \Delta K_{dj(k-1)}$.

If $e_{(k)} < 0, \Delta s < 0, \Delta K_{pj(k)} = K_3 \times \Delta K_{pj(k-1)}$.

If $e_{(k)} > 0, \Delta s < 0, \Delta K_{pj(k)} = K_4 \times \Delta K_{pj(k-1)}, \Delta K_{ij(k)} = I_4 \times \Delta K_{ij(k-1)}, \Delta K_{dj(k)} = D_4 \times \Delta K_{dj(k-1)}$.

In other cases, the parameters remain unchanged.

where $K_{pj(k)} = K_{pj(k-1)} + \Delta K_{pj(k)}$, $K_{ij(k)} = K_{ij(k-1)} + \Delta K_{ij(k)}$, $K_{dj(k)} = K_{dj(k-1)} + \Delta K_{dj(k)}$; K_1, K_2, K_3, K_4, I_2, I_4, D_2, *and* D_4 are constants set according to the experience and knowledge of experts.

In the process of motor actuator movement, the current optimal control parameters are directly called according to the stage of the motor actuator, which saves calculation and analysis time, ensuring that the system controls the motor movement quickly and accurately.

To further strengthen the rapidity and anti-interference capability of the control strategy, the feedback principle is studied in depth. The basic function of the control strategy is to compare the controlled variable with the reference input and make decisions based on the error. The performance of the control system is determined by the operation and treatment of the errors using a control algorithm. A system block diagram of the conventional PID control algorithm is shown in Fig. 9.

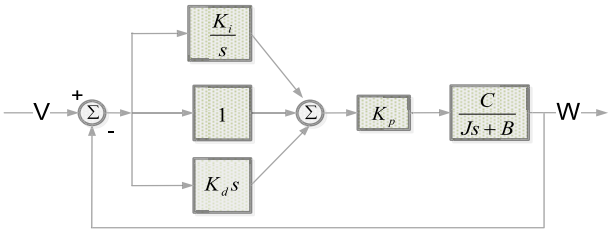

FIGURE 9. Block diagram of PID control strategy.

In the feed-forward loop, each error operation is added along with the operation on the reference input and controlled variable. Each operation on reference input will be shown in the differential equation of the whole control strategy, refer to"(1)":

$$\left(J + CK_pK_d\right)\frac{dw\,(t)}{dt} + \left(B + CK_p\right)w\,(t) + CK_pK_i\int w\,(t)dt = CK_pK_i\int v\,(t)\,dt + CK_pv\,(t) + CK_pK_d\frac{dv\,(t)}{dt} \quad (1)$$

where $C/(Js + B)$ is the controlled object *and* Kp, Ki, and Kd are the proportional, integral, and differential parameters, respectively. where w(t) is the output and v(t) is the input. As can be observed from the equation, there are three forcing terms on the right-hand side of the equation:

$$CK_pK_i\int v(t)dt + CK_pv(t) + CK_pK_d\frac{dv(t)}{dt} \quad (2)$$

This causes the output to not only follow the change in the input but also change with the integration and differentiation of the input.

According to the analysis, only the integral can be used in the feed-forward loop of the control strategy; however, to ensure ideal control characteristics, such as rapidity and stability, it is necessary to provide the differential of the controlled object. To avoid introducing the differential of the reference input, the differential of the controlled object for compensation purposes must be in the feedback loop. Based on the analysis above, a block diagram of the control strategy is presented in Fig. 10.

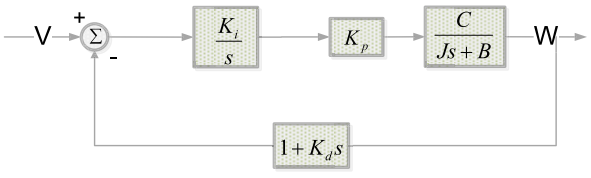

FIGURE 10. Block diagram of optimized PID control strategy.

The differential equation is:

$$J\frac{d^2w\,(t)}{dt^2} + \left(B + CK_pK_iK_d\right)\frac{dw\,(t)}{dt} + CK_pK_i = CK_pK_iv\,(t) \quad (3)$$

Fig. 10 shows that the output signal after operating the calculus is still w(t), which means that there is no need to differentiate w(t). In practice, differential operation should be avoided as much as possible. The optimization of the control strategy is illustrated in Fig. 11.

It's still going to be the derivative:

$$J\frac{d^2w\,(t)}{dt^2} + \left(B + CK_pK_iK_d\right)\frac{dw\,(t)}{dt} + CK_pK_i = CK_pK_iv\,(t) \quad (4)$$

Without differentiating the controlled variables directly, the obtained results are exactly the same as those obtained by differentiating to ensure that the system has a fast response capability and anti-interference ability.

The control algorithm was combined with a motor model to build the system model. Analyze the mathematical model of the motor and assume that

The influence of stator winding groove on motor magnetic field is ignored.

It is assumed that the power elements in the drive circuit are ideal.

The electromagnetic field generated by the motor winding does not reach saturation, and energy is not lost.

The main magnetic field is produced by the permanent magnet, and the influence of the stator magnetic field can be ignored.

(5) can be obtained by analyzing the steady mathematical model of the motor.

$$u = 2Ri + 2(L - M)\frac{di}{dt} + E + \Delta U \quad (5)$$

where i is the motor current, E is the back EMF, *and* ΔU is the power inverter voltage drop.

The motion equation of the motor is:

$$T_e - T_L = J\frac{dw}{dt} + B_vw \quad (6)$$

where T_e denotes the electromagnetic torque, T_L denotes the load torque of the motor shaft, J denotes the rotational inertia of the motor shaft, B_v denotes the coefficient of viscosity, *and* w denotes the motor angular velocity.

By analyzing the working principle of the motor, torque pulsation and speed fluctuation exist; therefore, the dynamic model of the motor is a nonlinear system with strong coupling of multistage variables. However, the power-switching frequency of the driving motor is high. To better design the control system and analyze the control performance, the nonlinear changes in the current at the commutation time of the motor and the nonlinear transition process of the power-switching device can be linearized. For example, it can be assumed that the phase current changes, the transition process of the power switching components, and the influence of PWM voltage regulation on the current and torque are ignored. In this way, the Laplace transform of the above dynamic mathematical model can be performed to obtain the

second-order linear transfer function of the motor:

$$\frac{I_d(s)}{U_d(s) - E(s)} = \frac{1}{(L-M)s + 2R} \tag{7}$$

$$\frac{n(s)}{K_T I_d(s) - T_L(s)} = \frac{1}{Js + B_v} \tag{8}$$

where I_d is the average motor current, U_d is the DC bus voltage, L is the phase inductance, R is the phase resistance, M is the mutual inductance, n is the motor speed, *and* K_T is the motor torque constant. According to (7)and (8), the dynamic structure diagram of the motor model can be obtained as shown in Fig. 12.

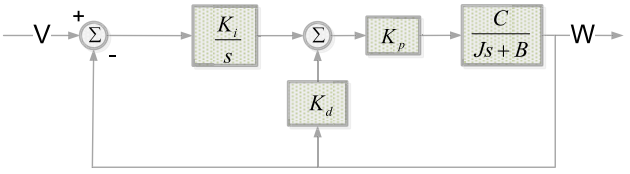

FIGURE 11. Block diagram of avoidance differential control strategy.

Owing to the working principle of the power amplifier inverter, when its control voltage changes, its output voltage can only be changed in the next cycle. Therefore, the entire power amplifier inverter is equivalent to a lag-amplification link. Through simplified analysis, the transfer function of the power amplifier inverter can be obtained as (9).

$$G_{PWM}(s) = \frac{U_d(s)}{U_c(s)} = \frac{K_s}{T_s s + 1} \tag{9}$$

where U_d is the DC bus voltage, U_c is the PWM control voltage, K_s is the amplification factor of the power amplifier inverter, and T_s is the switching cycle of the power amplifier inverter.

By integrating the motor transfer function model and the power amplifier inverter transfer function model, and taking the feedback link of current and speed as the proportional link, the dynamic structure diagram of the double closed-loop speed regulation system can be obtained, as shown in Fig. 13.

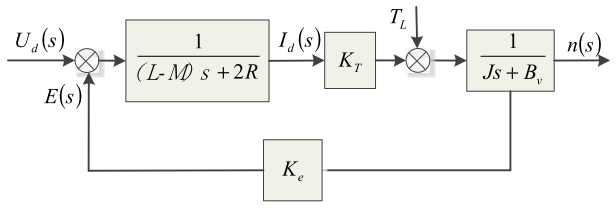

FIGURE 12. The dynamic structure diagram of the motor model.

where FPI is the function switch PI control, α is the feedback gain coefficient, and β is the current feedback gain coefficient.

According to the principle of automatic control, the transfer function of the PI control is

$$G_{PI}(s) = \frac{K_P(\tau_i s + 1)}{\tau_s s} \tag{10}$$

where K_P is the proportionality coefficient *and* τ is the integral time constant. The equivalent transfer functions of the speed and current loops are substituted in Fig. 13 for a simplified derivation, and the double-closed-loop dynamic structure of the motor control system can be obtained, as shown in Fig. 14.

B. THE SIMULATION ANALYSIS

A simulation analysis was performed to verify the effectiveness of the control algorithm designed in this study. The motor designed in this study is selected as the control object. The simulation model was constructed according to the analysis described in the previous section. The Simulink simulation block diagram of the speed FPD control strategy is shown in Fig. 15, and the Simulink simulation block diagram of the current FPI control strategy is shown in Fig. 16.

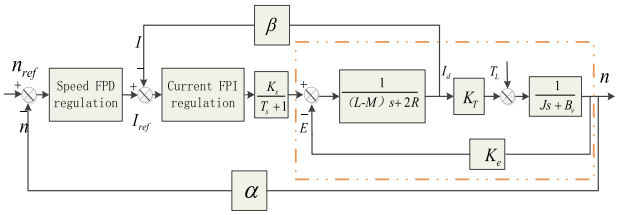

FIGURE 13. Dynamic structure of double closed loop speed control system.

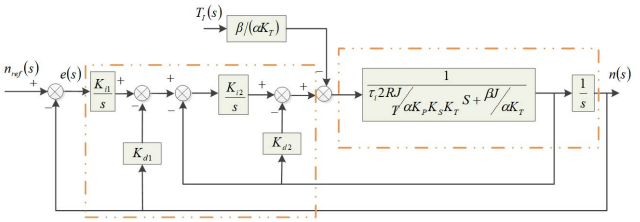

FIGURE 14. The further deduced dynamic structure of the double closed loop speed control system.

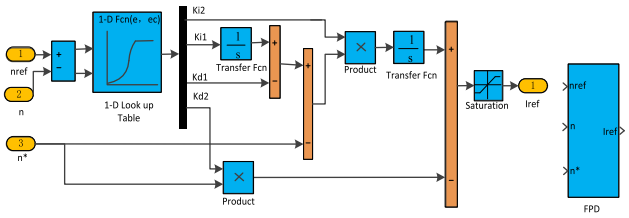

FIGURE 15. Simulink simulation block diagram of speed FPD control strategy.

During the closing of the VCB, the motor is in speed control mode, and the output torque changes with the load. The precision of realizing the zero-phase closing operation is mainly reflected in the response speed and anti-jamming of the motor. The fast response speed of the motor ensures its ability to follow the preset curve. Strong anti-interference

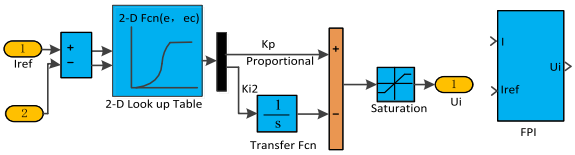

FIGURE 16. Simulink simulation block diagram of current FPI control strategy.

can ensure speed-following ability in the case of a torque change. Based on the above analysis, the response speed and anti-interference ability of the motor were simulated and analyzed. A conventional PID control strategy was selected for the comparative analysis. PID control parameters were selected according to operational experience and control rules. The control parameters were repeatedly verified experimentally as the optimal control parameters ($K_p = 0.33$, $K_i = 237.51$, $k_d = 6.85$). Fig. 17 shows the speed response curves of the FPD and conventional PID controls at a given preset speed.

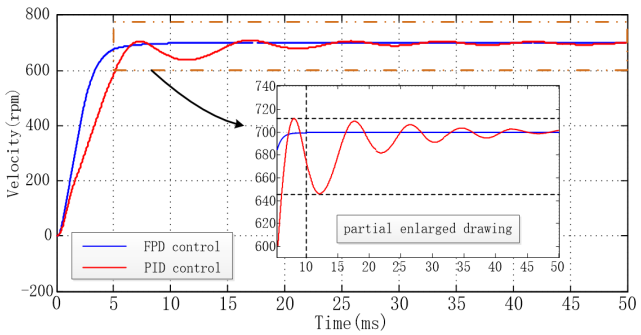

FIGURE 17. Speed response curve.

As shown in Fig. 17, the preset reference speed is set to 700rpm. Under the FPD control algorithm, the speed reaches the preset reference value, and the settling time is 10ms without an overshoot. Under the PID control algorithm, the stabilization time required to reach the preset reference value was 50ms, and the maximum overshoot was 1.4%. The simulation analysis shows that the speed response under FPD control is faster than that under PID control and without an overshoot.

The stability of the system was verified by considering that the motor changes with the load during the VCB closing. We set a constant speed and sudden torque, and compared the ability of the FPD control strategy and PID control strategy to adjust for sudden interference. Fig. 18 shows the anti-interference simulation curves for the two cases.

In the stable process of constant speed output of the control system, when t = 0.1s, the load is suddenly added, and the interfering load increases from 50 Nm to 300 Nm. The overshoot of the FPD control strategy was 1.67% and the recovery time was 1ms. The overshoot of the conventional PID control strategy is 8.33%, and the recovery time is 23ms.

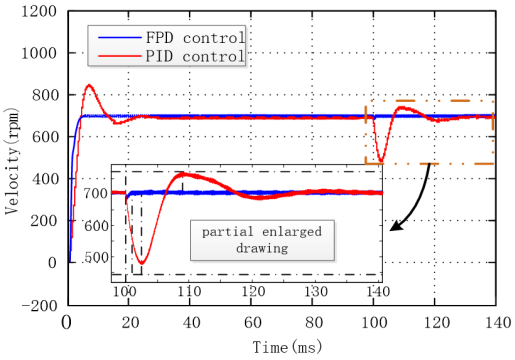

FIGURE 18. Anti-interference simulation curve.

The simulation showed that the FPD control strategy is more stable in the case of interference. This can ensure accurate control of the output speed under the condition of variable torque during operation.

The closing operation process of the VCB was simulated, the preset reference speed was set, and a speed-tracking simulation experiment was performed. The experimental results are shown in Fig. 19.

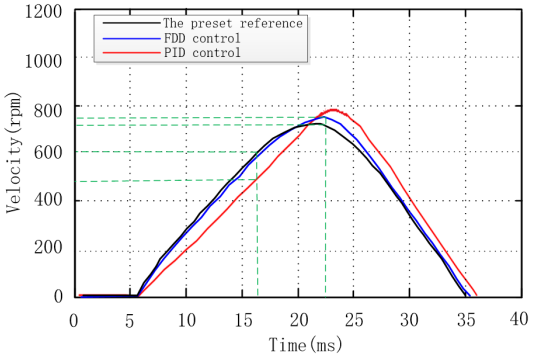

FIGURE 19. Velocity tracking simulation curve.

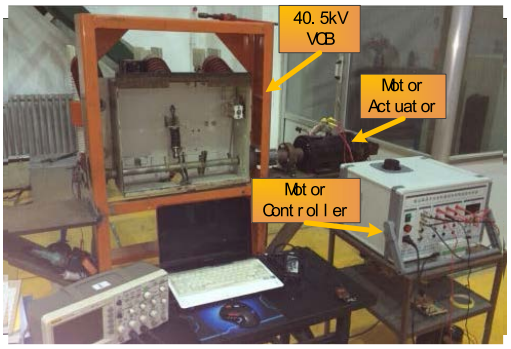

FIGURE 20. 40.5 kV VCB and motor actuator test site.

According to the simulation results, the entire tracking process was 30ms, and the preset reference speed gradually increased from 0, and began to decrease after reaching the maximum speed of 700rpm, and the speed was 0 at 35ms.

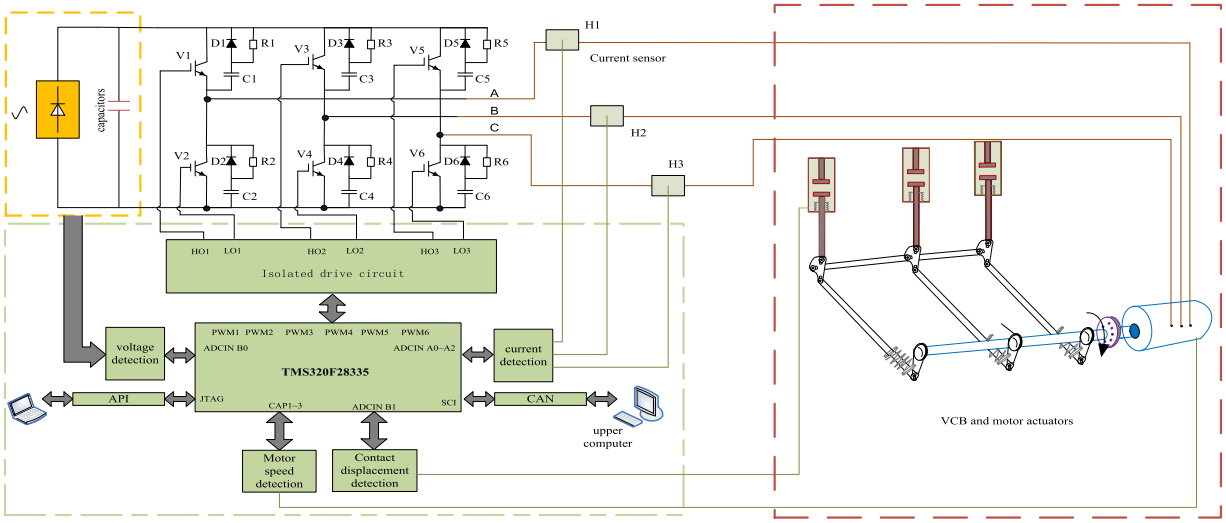

FIGURE 21. Structural block diagram of motor actuator speed regulation system.

The FPD control algorithm was adopted, and the tracking error was controlled within 10rpm before the maximum speed was reached, and the maximum tracking error was 34.2 rpm after the maximum speed was reached. With the conventional PID control algorithm, the tracking error was obvious before reaching the maximum speed, and the maximum tracking error was 114.8 rpm. After reaching the maximum speed, the tracking error decreased; however, the error value was greater than 10 rpm.

Therefore, the performance of the VCB motor actuator using the FPD control algorithm was better than that of the PID control algorithm.

IV. CONTROL SYSTEM DEVELOPMENT AND EXPERIMENTAL VERIFICATION

A. DESIGN OF CONTROL SYSTEM

To verify the effectiveness of the new control strategy in the drive control application of the VCB motor actuator, a drive motor was developed, a 40.5 kV VCB motor actuator and its control system were built. A specific physical experimental site is shown in Fig. 20. The FPD and conventional PID control strategies were compared on the same hardware platform of the control system.

The hardware platform structure diagram of the control system is shown in Fig. 21. The control system used DSP28335 as the core data processing unit, with a power module, signal acquisition module, IGBT, drive module, capacitor charge and discharge module, CAN communication, and an upper computer. To ensure control accuracy, high-precision sensors are used for signal acquisition, such as current, speed, and contact position, and the control system adopts three closed-loop control strategies: position, speed, and current loops.

B. EXPERIMENTAL VERIFICATION

The accuracy of the zero-phase closing operation of the VCB is primarily reflected by the fact that the speed of the switch contact can accurately follow the calculated preset reference speed. The velocity-following experiment was selected to verify the effectiveness of the new control algorithm. Fig. 22 shows the curve of the experimental data.

According to the comparison between a) and b) in Fig. 22, it can be seen that the speed rising stage of the switch moving contact is its travel stage, and the speed tracking error under the conventional control algorithm is 0.3 m/s, while that under the new control algorithm is 0.08 m/s. When the speed of the moving contact reaches the maximum stage, in order to overcome the counterforce, the tracking errors of the two increases, which are 0.55 m/s and 0.2 m/s respectively. In the deceleration stage, the spring is compressed after the dynamic and static contacts of the VCB; meanwhile, the preset speed curve exhibits a large change rate. At this time, the tracking errors of the two are 0.5 m/s and 0.15 m/s respectively.

The simulation results of the speed-tracking experiments were analyzed, and the motor speed in the simulation results was converted to the switch contact side. The maximum error of the motor speed of the FPD algorithm is 34.2 rpm, and the speed tracking error of the corresponding switch contact is 0.086 m/s. The maximum error of the PID algorithm was 114.8r/min, and the speed tracking error of the corresponding switch contact was 0.282 m/s. In the zero-phase closing experiment, the maximum tracking error of switch contact speed under FPD algorithm is 0.2 m/s, and the maximum tracking error of switch contact speed under PID algorithm is 0.55 m/s. Comparing the simulation results with the experimental results, there is a certain deviation between the two results, but both results indicate that the FPD algorithm is better than the PID algorithm.

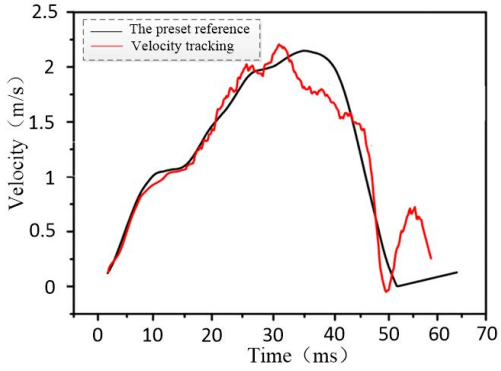

a) Switch contact speed follows the curve under conventional PID control

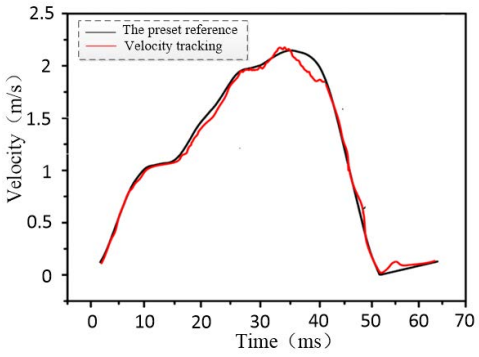

b) Contact speed follows the curve under the FPD control

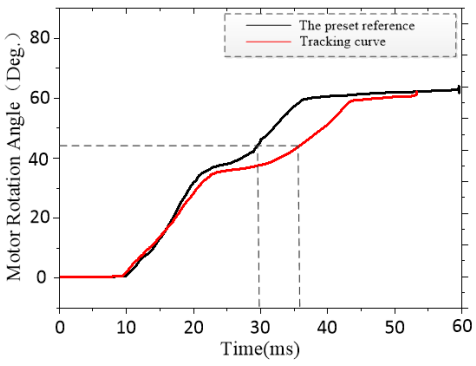

c) Motor rotation Angle following curve under conventional PID control

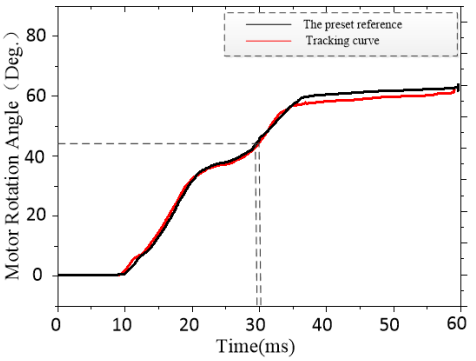

d) Motor rotation angle following curve under the FPD control

FIGURE 22. Comparison o switch contact velocity and motor rotation angle curve in VCB closing process under FPD and PID control.

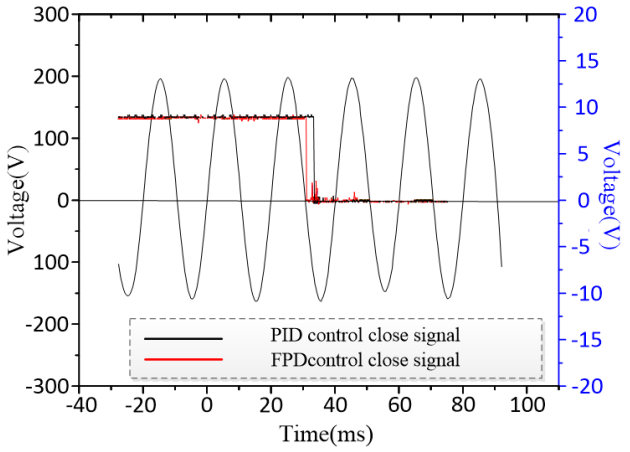

FIGURE 23. Zero-phase closing curve under FPD and PID control.

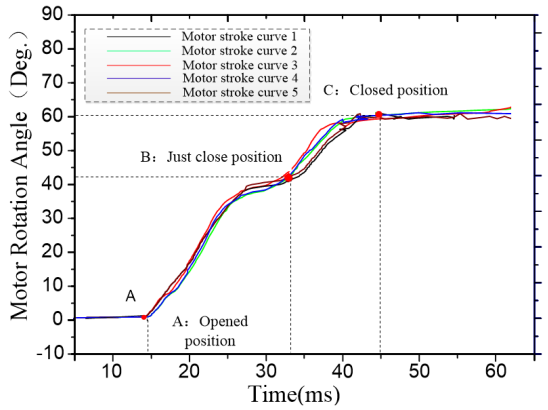

a) Motor rotation angle curve

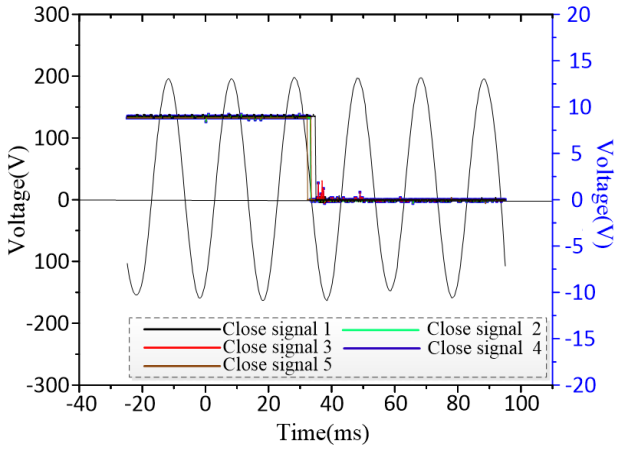

b) Closing signal curve

FIGURE 24. Curve of zero-phase closing repeatable experiment.

corresponding to the rotation angle of the motor. The experimental curves are shown in Fig. 19(c) and (d). Compared with the FPD control algorithm, the tracking deviation of the motor angle stroke under the PID control algorithm was larger. When the motor rotation angle was 42°, it was the contact time between the dynamic and static contacts. The following error is 6.2ms under the control of the conventional PID control algorithm, and which is 0.13ms under the control of the FPD control algorithm. A comprehensive analysis

shows that the speed-following performance of the motor actuator controlled by the new control strategy is better than that of the conventional control algorithm.

To intuitively demonstrate that the FPD control strategy can improve the phase-controlled closing accuracy, a zero-phase closing experiment was selected for verification. A 9V high level signal is applied to both ends of the VCB, which is pulled down when the VCB is closed. Fig. 23 shows the zero-phase closing curve under FPD and PID control. The difference between the VCB closing time and the grid voltage zero is 0.15ms under the FPD control strategy. The difference was 4.2ms under the PID control strategy.

To analyze the stability of the new control algorithm controlling the motor actuator to realize the zero-phase closing action of the VCB, a zero-phase closing repeatability experiment was carried out in this study. During the experiment, the experimental environment and conditions were kept unchanged, and the action was performed five times, consecutively. The experimental results after collecting and processing the experimental data are shown in Fig. 24.

In the motor motion travel curve in Fig. 24a), point A is the open position, point B is the just close point, and point C is the closed position. A - B are the travel stages during which the motor actuator rotates by 42°. B-C is the overtravel stage, where the motor actuator rotates by 20°. As shown in Fig. 24(a), the motor actuator drives the switch in stages A to B, and the motion trajectory has a high repetition rate. The closing time at point B is 33.36 ms, 33.60 ms, 33.61 ms, 33.78 ms, and 33.94 ms, respectively. In the B - C overtravel stage, the motor actuator continued to move. Because the spring reaction force needs to be overcome, the movement trajectory appears to have a certain dispersion. The entire closing process was completed at point C. Because point B is the just close position, the dynamic and static contact, and the closing signal mutates, the operation process of stages B - C does not affect the time stability of zero-phase closing.

As can be seen from the curve of the just close position in Fig. 24b), the closing at the sixth zero point in the figure was achieved for five consecutive experiments, and the time at the sixth zero point was 33.6ms. Compared with the closing experiment results at point B, the errors of the five experiments were -0.24ms, 0ms, 0.01ms, 0.18ms, and 0.34ms, respectively. The closing time error at zero crossing of the VCB is within ±0.5ms, which meets the operation precision requirements of CIGRE for phase-control closing technology.

V. CONCLUSION

This study proposes an FPD control strategy for the motor actuator control system of a VCB. It has the characteristics of fast response ability and strong anti-interference ability, which is suitable for a VCB motor actuator control system with a short movement time and complex environment. From the simulation and the experiment of the VCB, we can draw the following conclusions: 1) Under the FPD control algorithm, the speed reaches the preset reference value, and the settling time is 10ms without overshoot. Under the PID control algorithm, the stabilization time required to reach the preset reference value was 50ms, and the maximum overshoot was 1.4%. The FPD control algorithm is rapid. 2) Under interference, the overshoot of the FPD control strategy was 1.67%, and the recovery time was 1ms. The overshoot of the conventional PID control strategy is 8.33%, and the recovery time is 23ms. The simulation showed that the FPD control strategy is more stable in the case of interference. 3) From the experiment of zero-phase closing of VCB, the FPD control strategy was verified to be able to accurately control the action of the motor actuator driving the contact, and realize a contact closing time error within ±0.5 ms, with stability.

REFERENCES

[1] J. Lou, A. Liu, and S. Yu, "A reliable and controllable motor actuator without permanent magnetic for 40.5 kV vacuum circuit breakers," *IEEE Trans. Ind. Appl.*, vol. 56, no. 2, pp. 1218–1225, Dec. 2019.

[2] Z. Wang, L. Sun, S. He, Y. Geng, and Z. Liu, "A permanent magnetic actuator for 126 kV vacuum circuit breakers," *IEEE Trans. Magn.*, vol. 50, no. 3, pp. 129–135, Mar. 2014.

[3] X. Pei, A. C. Smith, R. Shuttleworth, D. S. Vilchis-Rodriguez, and M. Barnes, "Fast operating moving coil actuator for a vacuum interrupter," *IEEE Trans. Energy Convers.*, vol. 32, no. 3, pp. 931–940, Sep. 2017.

[4] B. Zhang, Y. Tan, L. Ren, J. Wang, Y. Geng, Z. Liu, and S. Yanabu, "Interruption capability of a fast vacuum circuit breaker with a short arcing time," in *Proc. 27th Int. Symp. Discharges Electr. Insul. Vac. (ISDEIV)*, Sep. 2016, pp. 1–4.

[5] T. Wang, J. Yan, X. Zhai, Z. Liu, Y. Geng, and Y. Chen, "Research on 40.5 kV Two-break vacuum circuit breaker for switching capacitor banks," in *Proc. 27th Int. Symp. Discharges Elect. Insul. Vac.*, Suzhou, China, Sep. 2016, pp. 1–4.

[6] J. Zhao, M. Hua, and T. Liu, "Cooperative optimization and fault-tolerant control method of multi-disk permanent magnet synchronous motor for electric vehicles," *Proc. CSEE*, vol. 39, no. 2, p. 9, 2019.

[7] A. V. Sant, K. R. Rajagopal, and N. K. Sheth, "Permanent magnet synchronous motor drive using hybrid PI speed controller with inherent and noninherent switching functions," *IEEE Trans. Magn.*, vol. 47, no. 10, pp. 4088–4091, Oct. 2011.

[8] S. Niu, Y. Luo, W. Fu, and X. Zhang, "Robust model predictive control for a three-phase PMSM motor with improved control precision," *IEEE Trans. Ind. Electron.*, vol. 68, no. 1, pp. 838–849, Jan. 2021.

[9] A. K. Junejo, W. Xu, C. Mu, M. M. Ismail, and Y. Liu, "Adaptive speed control of PMSM drive system based a new sliding-mode reaching law," *IEEE Trans. Power Electron.*, vol. 35, no. 11, pp. 12110–12121, Nov. 2020.

[10] J. Vittek, V. Vavrus, M. Malek, P. Buchner, and W. Michalik, "Prescribed closed-loop speed dynamics control of the actuator employing linear permanent magnet synchronous motor," in *Proc. IEEE Int. Conf. Ind. Technol.*, Dec. 2006, pp. 604–609.

[11] M. F. Rahman, L. Zhong, and K. W. Lim, "A direct torque controlled interior permanent magnet synchronous motor drive incorporating field weakening," in *Proc. Conf. Rec. IEEE Ind. Appl. Conf. 32nd IAS Annu. Meeting (IAS)*, Oct. 2002, pp. 67–74.

[12] M. Konghirun and L. Xu, "A fast transient-current control strategy in sensorless vector-controlled permanent magnet synchronous motor," *IEEE Trans. Power Electron.*, vol. 21, no. 5, pp. 1508–1512, Sep. 2006.

[13] A. Wang, X. Jia, and S. Dong, "A new exponential reaching law of sliding mode control to improve performance of permanent magnet synchronous motor," *IEEE Trans. Magn.*, vol. 49, no. 5, pp. 2409–2412, May 2013.

[14] A. Nasiri, "Full digital current control of permanent magnet synchronous motors for vehicular applications," *IEEE Trans. Veh. Technol.*, vol. 56, no. 4, pp. 1531–1537, Jul. 2007.

[15] H. P. Ren and D. Liu, "Nonlinear feedback control of chaos in permanent magnet synchronous motor," *IEEE Trans. Circuits Syst. II, Exp. Briefs*, vol. 53, no. 1, pp. 45–50, Jan. 2006.

[16] H. Nakai, H. Ohtani, E. Satoh, and Y. Inaguma, "Development and testing of the torque control for the permanent-magnet synchronous motor," *IEEE Trans. Ind. Electron.*, vol. 52, no. 3, pp. 800–806, Jun. 2005.

[17] B. Cheng and T. R. Tesch, "Torque feedforward control technique for permanent-magnet synchronous motors," *IEEE Trans. Ind. Electron.*, vol. 57, no. 3, pp. 969–974, Mar. 2010.
[18] P. Gao, G. Zhang, H. Ouyang, and L. Mei, "An adaptive super twisting nonlinear fractional order PID sliding mode control of permanent magnet synchronous motor speed regulation system based on extended state observer," *IEEE Access*, vol. 8, pp. 53498–53510, 2020.
[19] A. V. Sant and K. R. Rajagopal, "PM synchronous motor speed control using hybrid fuzzy-PI with novel switching functions," *IEEE Trans. Magn.*, vol. 45, no. 10, pp. 4672–4675, Oct. 2009.
[20] H. H. Choi, H. M. Yun, and Y. Kim, "Implementation of evolutionary fuzzy PID speed controller for PM synchronous motor," *IEEE Trans. Ind. Informat.*, vol. 11, no. 2, pp. 540–547, Apr. 2015.
[21] Y. Huang, J. Wang, W. Zhang, M. Al-Dweikat, D. Li, T. Yang, and S. Shao, "A motor-drive-based operating mechanism for high-voltage circuit breaker," *IEEE Trans. Power Del.*, vol. 28, no. 4, pp. 2602–2609, Oct. 2013.
[22] K. Qu, J.-Y. Xu, G.-N. Wu, and X. Jin, "Research on speed control method of motor operated mechanism of 126 kV vacuum circuit breaker," in *Proc. 4th Int. Conf. Electr. Power Equip. Switching Technol. (ICEPE-ST)*, Oct. 2017.
[23] A. Liu, Y. Bi, Z. Wu, and Y. Yang, "Design of permanent magnet motor actuator and control system for high voltage circuit breaker," *Electr. Mach. Control J.*, vol. 19, no. 1, p. 6, 2015.

AIMIN LIU (Member, IEEE) was born in Liaoning, China, in 1961. She received the Ph.D. degree in electrical engineering from the Shenyang University of Technology, Shenyang, China, in 2009. Since 1992, she has been a Lecturer with the School of Electrical Engineering, Shenyang University of Technology, where she has been currently a Professor, since 2019. Her teaching activities and research interests include power electronics and power transmission, electric machines, and electric apparatus.

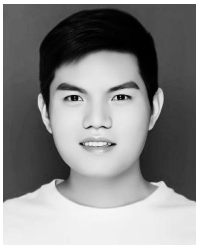

ZHIHENG WU (Member, IEEE) received the B.S. degree in electrical engineering from Liaoning Shihua University, Liaoning, China, in 2012, and the M.S. degree in electrical engineering from the Shenyang University of Technology, Shenyang, China, in 2015, where he is currently pursuing the Ph.D. degree in electrical engineering. His research interests include electrical machine design, design optimization, modeling and analysis of electric machines, and control of electrical machines.

YUCHEN WANG (Member, IEEE) received the B.S. and M.S. degrees in electrical engineering from the Shenyang University of Technology, Shenyang, China, in 2016 and 2021, respectively, where he is currently pursuing the Ph.D. degree in electrical engineering. His research interests include power generation system design, electrical machine design, and control of electrical machines.

SHAOHUA MA (Member, IEEE) received the bachelor's and Ph.D. degrees in electrical engineering from the Shenyang University of Technology, in 1988 and 2008, respectively. She is currently a Professor with the College of Electrical Engineering, Shenyang University of Technology. Her research interests include intelligent electrical apparatus, advanced digital control technique, and power electronics applications in power systems.